Noname manuscript No.
(will be inserted by the editor)

Fluid-solid transition in unsteady, homogeneous, granular shear flows

Dalila Vescovi · Diego Berzi · Claudio di Prisco

Received: date / Accepted: date

Abstract Discrete element numerical simulations of unsteady, homogeneous flows have been performed by shearing a fixed volume of identical, soft, frictional spheres. A constant, global, shear rate was instantly applied to particles that are initially at rest, non interacting, and randomly distributed. The granular material exhibits either large or small fluctuations in the evolving pressure, depending whether the average number of contacts per particle (coordination number) is less or larger than a critical value. When the coordination number is less than the critical value, the amplitude of the pressure fluctuations is dependent on the shear rate, whereas, it is rate-independent in the opposite case, signatures, according to the case, of fluid-like and solid-like behaviour. The same critical coordination number has been previously found to represent the minimum value at which rate-independent components of stresses develop in steady, simple shearing and the jamming transition in isotropic random packings. The observed complex behaviour of the measured pressure in the fluid-solid transition can be predicted with a constitutive model involving the coordination number, the particle stiffness and the intensity of particle agitation.

Keywords Fluid-solid transition · Unsteady flows · Numerical simulations

1 Introduction

Granular materials exhibit a complex mechanical behaviour, even in the case of simple flow conditions, whose study involves interdisciplinary concepts like rheology, plasticity and viscosity.

Depending on both the micro-mechanical properties of the grains (surface friction, collisional inelasticity and contact stiffness) and the macroscopic characteristics of the flow (e.g., velocity and bulk density), different flow regimes exist. Consider, for example, a landslide: immediately after the triggering, it behaves like a solid and a sliding motion takes place; but, if its velocity is sufficiently large, the landsliding evolves into a fluid-like process.

When the system is extremely dense, enduring contacts among grains involved in force chains govern its response, which is mainly rate-independent [8]. In this case, a stable contact network develops within the medium [16] and the granular material behaves like a solid, able to resist finite applied shear stresses without deforming.

On the other hand, when the particles are widely spaced, force chains are inhibited and collisions dissipate the energy of the system. As a consequence, the medium is strongly agitated and the particles are free to move in all directions [14]. The material response is that of a fluid, that is it yields under shear stress, and stresses are rate-dependent.

The mechanical response of the system during the solid-fluid transition is still an open question [25], although several constitutive models have been proposed in the literature to deal at least with steady flow configurations [3, 8, 20, 35, 41, 42].

Molecular dynamics simulations based on Discrete Element Method (DEM) have been successfully employed to study granular systems under different flow regimes, configurations and geometries (collections of results can be found in [13] and in [10]). Whereas several numerical results in the literature concern steady,

D. Vescovi - D. Berzi - C. di Prisco
Department of Civil and Environmental Engineering, Politecnico di Milano, 20133 Milano, Italy
Tel.: +39-02-23996262
E-mail: dalila.vescovi@polimi.it

shearing granular flows [2, 6, 7, 8, 9, 11, 19, 29, 41], unsteady conditions have been less investigated.

Sun and Sundaresan [39] carried out DEM simulations of unsteady, homogeneous shear flows of frictional spheres at constant solid volume fraction. They focused on the solid regime, where the stresses are rate-independent, and showed that, in that case, the pressure scales with the product of the particle stiffness and the square of the distance of the coordination number, i.e., the average number of contacts per particle, from a critical value.

Here, DEM simulations of unsteady, homogeneous, shear flows of identical, frictional spheres under constant volume allow to investigate the fluid-solid transition. The instantaneous application of a constant shear rate to a random, static collection of non-interacting particles (zero initial pressure) forces the system to evolve towards a steady state, while keeping constant the solid volume fraction. A fluid-solid transition governed by the coordination number is observed for specific values of the imposed solid volume fraction. There, the pressure does not obey the simple scaling relation observed in the solid regime [39].

Section 2 describes the DEM numerical simulations performed and the specimen preparation procedure. The results of the simulations are thoroughly discussed in Section 3, while Section 4 provides some concluding remarks.

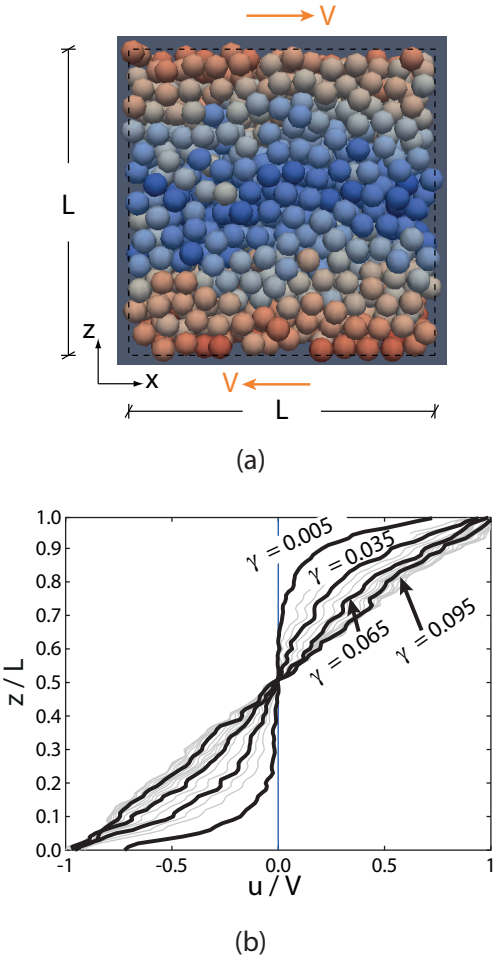

Fig. 1 (a) Sketch of the flow configuration. Grey intensity indicates speed, from dark grey (blue online) -zero velocity of the particles in the core of the domain- to light grey (red online) -maximum velocity of the particles at the boundaries. (b) Temporal evolution of the horizontal velocity profiles for shear flow of a $L = 12d$ granular system at a volume fraction $\nu = 0.59$ and (dimensionless) shear rate $\dot{\gamma}^* = \dot{\gamma}\sqrt{\rho_p d^3/k_n} = 3.16 \cdot 10^{-5}$, from an initial static state

2 DEM numerical simulations

We have performed DEM numerical simulations of unsteady, homogeneous shear flows of identical, frictional spheres using the open-source code Mercury-DPM [1] [40, 43] which models the particle-particle interaction with a linear spring-dashpot contact model. The normal force between particles at contact is $\mathbf{f}_{ij}^n = k_n \delta_{ij}^n \mathbf{n}_{ij} - \gamma_n \mathbf{v}_{ij}^n$, where δ_{ij}^n is the normal overlap between particles, k_n is the normal spring constant, γ_n is the damping coefficient, $\mathbf{n}_{ij}$ is the normal unit vector and $\mathbf{v}_{ij}^n$ is the normal relative velocity. Likewise, the tangential force is $\mathbf{f}_{ij}^t = -k_t \delta_{ij}^t \mathbf{t}_{ij} - \gamma_t \mathbf{v}_{ij}^t$, where k_t is the tangential spring constant, δ_{ij}^t the tangential overlap, γ_t the tangential damping, $\mathbf{t}_{ij}$ the tangential unit vector and $\mathbf{v}_{ij}^t$ the tangential velocity at the contact point in the case of small overlap. The tangential overlap is set to zero at the initiation of a contact and its rate of change is given by the tangential relative velocity. The rigid body motion around the contact is taken into account to ensure that the tangential displacement always belongs to the local tangent plane of the contact [24, 26]. The magnitude of δ_{ij}^t is truncated as necessary to satisfy Coulomb law, i.e., $\left|\mathbf{f}_{ij}^t\right| \leq \mu \left|\mathbf{f}_{ij}^n\right|$, where μ is the inter-particle friction coefficient. The static friction coefficient is constant and equal to its dynamic counterpart. In this simplified framework, the contacts are sticking if $\left|\mathbf{f}_{ij}^t\right| < \mu \left|\mathbf{f}_{ij}^n\right|$ and sliding if $\left|\mathbf{f}_{ij}^t\right| = \mu \left|\mathbf{f}_{ij}^n\right|$.

The coefficients of normal and tangential restitution, e_n and e_t, which relate the pre-collisional and post-collisional normal and tangential relative velocities, characterize the collisions. For the linear spring-dashpot model, the following relationships between the coefficients of restitution, the spring constants and the

[1] www.mercurydpm.org

damping coefficients hold [37]:

$$\gamma_n = \sqrt{\frac{4m_p k_n \left(\log e_n\right)^2}{\pi^2 + \left(\log e_n\right)^2}};$$
$$\gamma_t = \sqrt{\frac{2}{7}\frac{4m_p k_t \left(\log e_t\right)^2}{\pi^2 + \left(\log e_t\right)^2}};$$
$$k_t = \frac{2}{7}k_n \frac{\pi^2 + \left(\log e_t\right)^2}{\pi^2 + \left(\log e_n\right)^2}, \quad (1)$$

where m_p is the particle mass.

The evolution with time t of particle pressure p, coordination number Z and granular temperature T (one third of the mean square of the particle velocity fluctuations, a measure of the pseudo-thermal agitation of the particles [18]), is measured for different shear rates $\dot{\gamma}$ and volume fractions. For a granular material, the solid volume fraction is defined as the ratio of the particle mass density to the bulk density. To extract the macroscopic fields we use the spatial coarse-graining approach described in details in Weinhart et al. [43, 44]. In particular, the pressure is defined as $p = \mathrm{tr}\left(\boldsymbol{\sigma}\right)/3$, where $\boldsymbol{\sigma}$ is the stress tensor, calculated as the sum of the kinetic (or streaming) and the contact contribution.

2000 particles of diameter d and density ρ_p are placed in a cubic box of dimension L (Fig. 1a). The size L of the domain depends on the desired solid volume fraction ν. In all simulations, the normal coefficient of restitution e_n is equal to 0.7, the tangential spring stiffness k_t is equal to 2/7 k_n (implying $e_t = e_n = 0.7$) and the friction coefficient μ is assumed equal to 0.3. Lees-Edwards [22] periodic boundary conditions along z (velocity gradient direction) and periodic boundary conditions along x and y (flow and vorticity directions, respectively) force the system to be homogeneous in space after a short transient. Due to some difficulties of coarse-graining in the proximity of Lees-Edwards boundaries, measurements in regions of thickness 2 to 3 diameters at the top and the bottom of the cubic box are not considered. The relative motion of the planar boundaries perpendicular to z, at constant velocity $2V$, shears the system at a global shear rate $\dot{\gamma} = 2V/L$. The integration time step is set equal to $t_c/50$, where the collisional time for the spring-dashpot contact model is $t_c = \{\rho_p \pi d^3[\pi^2 + (\log e_n)^2]/(12k_n)\}^2$. The saving time step of the simulations is set so that measurements are recorded at intervals of $0.001/\dot{\gamma}$.

The instantaneous application of a relative velocity between the boundaries is not immediately transmitted within the entire granular material. As a consequence, the velocity profiles are initially non linear; the local shear rate is not homogeneous, but is maximum at the boundaries and minimum (close to zero) in the core. After a short time interval ($0 < \gamma < 0.07$, where $\gamma = \dot{\gamma}t$ is the accumulated shear strain, or, equivalently, a dimensionless time) the inhomogeneity vanishes, and the velocity profiles become linear. Fig. 1(b) shows an example of the temporal evolution of the velocity profiles $u(z)$ along x. Unlike other numerical simulations [1], crystallization was never observed.

Simulations have been performed for three values of the constant solid volume fraction ν: 0.59, 0.60 and 0.62. In the case of steady, homogeneous shear flows, the volume fraction determines whether the granular system is solid-like or fluid-like, with the phase transition occurring at the critical volume fraction ν_c -the largest volume fraction at which a random assembly of granular material can be sheared without developing rate-independent contributions to the stresses [8]. The critical volume fraction depends on poly-dispersity [21, 30] and friction [8]: for identical particles with $\mu = 0.3$, ν_c is 0.596 [8]. Hence, after reaching the steady state, our three specimens are in fluid ($\nu = 0.59$), solid ($\nu = 0.62$) and near-to-critical ($\nu = 0.60$) conditions. At the steady state, there is a one-to-one relation between the critical volume fraction and the critical coordination number Z_c, independent of the shear rate [39, 41]. The coordination number Z is an important parameter to describe the granular interaction at large volume fractions, when force chains develop [19].

Here and in the following, the variables are made dimensionless by using the particle diameter d, density ρ_p and normal stiffness k_n. Then, the dimensionless pressure, granular temperature and shear rate are, respectively, $p^* = pd/k_n$, $T^* = Td\rho_p/k_n$ and $\dot{\gamma}^* = \dot{\gamma}\sqrt{\rho_p d^3/k_n}$. In particular, the dimensionless shear rate represents the ratio of the rate of shearing to the rate of relaxation of two particles under their repulsive potential.

2.1 Preparation

The preparation of the system follows a standard three-step procedure [17, 21]:

(i) 2000 frictionless spherical particles of diameter d and density ρ_p are randomly placed with random velocities in the 3D cubic box of initial size L_0 at moderate volume fraction ν_0 (where $\nu_0 = 2000\pi d^3/6L_0^3$), such that they have sufficient space to exchange places and randomize themselves. At the end of step (i), a static granular gas having zero pressure and coordination number is obtained.

(ii) The frictionless granular gas is then isotropically compressed to the target volume fraction ν. The cubic box reduces from size L_0 to $L = \left(2000\pi d^3/6\nu\right)^{1/3}$.

(iii) Finally, the particles are allowed to relax at constant volume fraction ν to dissipate their kinetic energy. In order to shorten the relaxation process, an artificial dissipation force, proportional to the velocity of the particles, is added, mimicking the damping due to a background medium, such as a viscous fluid.

At the end of the three stages, an isotropic, static granular specimen of volume fraction ν, with zero coordination number and zero pressure (athermal gas) is generated. During stage (ii), both the coordination number and the pressure increase from zero to a certain value, then, Z and p^* quickly drop to zero during stage (iii). At the end of the preparation procedure, the friction μ is set to 0.3, and the velocities at the boundaries are switched on so that the global shear rate $\dot{\gamma}$ has the desired value, constant in time.

3 Results

This Section describes the results of the DEM simulations. First, the mechanical quantities governing the phase transition in granular materials under both static and dynamic conditions (the latter being either steady or unsteady), are defined. In order to evaluate the critical coordination number under steady conditions, a set of steady numerical simulations has been performed by employing the same parameters introduced before, but for a larger range of volume fractions and shear rates. Then, the fluid-solid transition in the unsteady regime is analysed in terms of evolution of coordination number, pressure and granular temperature with the accumulated shear strain $\gamma = \dot{\gamma}t$, by considering three volume fractions and a fixed dimensionless shear rate. Different shear rates at sufficiently large volume fractions are also employed to show the rate-independency once the granular material solidifies. Finally, a constitutive model for the pressure, able to capture both fluid and solid conditions, is proposed.

3.1 Phase transition and critical coordination number

The fluid-solid transition in granular materials has been studied in the literature in both static and dynamic conditions, with different protocols [4, 8, 15, 23, 28, 31, 33, 36, 38, 39].

In isotropic, static conditions, the transition from a zero pressure state to a nonzero pressure state is known as jamming transition [23, 36, 38]. Isotropic granular packings, characterized by nonzero pressure and coordination number, are jammed structures, with a contact network percolating in all directions. The jamming transition is defined as a mechanical stable state characterized by zero pressure and finite coordination number, occurring when the system approaches a critical solid volume fraction ν_J (minimum volume fraction at which a random isotropic packing exists), whose value depends on the preparation history of the packing [36]. Moreover, there is a relation between ν_J and the coordination number at the jamming transition, Z_J. The effect of friction on the transition has been numerically investigated by approaching the jamming from below (i.e., isotropically compressing an athermal granular gas [38]) and from above (i.e., isotropically decompressing a random packing [36]). The results of the two procedures qualitatively agree and show that both the volume fraction and the coordination number at the jamming transition monotonically decreases with increasing friction. Transitions to anisotropic jammed states have been experimentally revealed for frictional particles subject to pure shear. These transitions seem to be governed by both shear stress and solid volume fraction [4].

In the case of steady, homogeneous shearing flows, Chialvo et al. [8] have measured the critical volume fraction ν_c at which rate-independent components of the stresses develop, based on the observation that the pressure fluctuations peak at that transition. Sun and Sundaresan [39] identified the critical coordination number Z_c governing the same transition by extrapolation to zero of the relation between the pressure and the coordination number. Simple fitting expressions [39] provide the dependence of both ν_c and Z_c on the friction coefficient:

$$\nu_c = 0.582 + 0.058\exp(-5\mu); \tag{2}$$

$$Z_c = 4.15 + 1.85\exp(-5\mu). \tag{3}$$

In the same case of steady, homogeneous shearing flows, Ji and Shen (for frictional spheres with $\mu = 0.5$ [19]) and Vescovi and Luding (for frictionless spheres [41]) have studied the dependence of the coordination number on the volume fraction, for different values of the dimensionless shear rate $\dot{\gamma}^*$ (or, equivalently, the dimensionless particle stiffness). Curves at different $\dot{\gamma}^*$ intersect at a critical point ν_c-Z_c, which is in excellent agreement with the fitting expressions of Eqs. (2) and (3).

Even if the goal of the present work is to analyse the phase transition under unsteady conditions, a set of simulations at the steady state has been performed with the aim of evaluating the critical coordination number. As already mentioned, in the steady simulations, the same boundary conditions and mechanical parameters described in Section 2 have been adopted. Fig. 2 shows the coordination number as a function of the solid volume fraction obtained in the present simulations of

steady, homogeneous shear flows for different values of the dimensionless shear rate when $\mu = 0.3$. The steady values of Z have been obtained by averaging in time over at least 1000 time steps. All the curves intersect at $\nu_c \approx 0.596$, with $Z_c \approx 4.6$. Once again, these values are in good agreement with Eqs. (2) and (3).

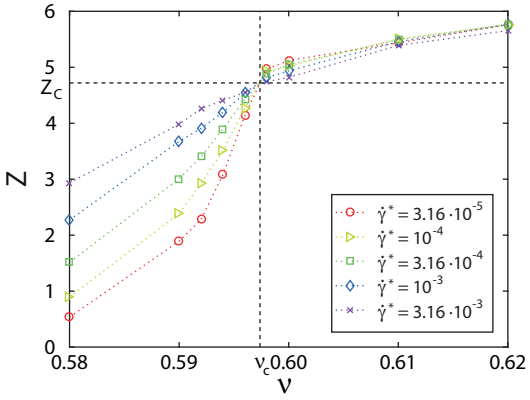

Fig. 2 Coordination number versus solid volume fraction in steady, homogeneous shear flows with $\mu = 0.3$ and different values of the dimensionless shear rate

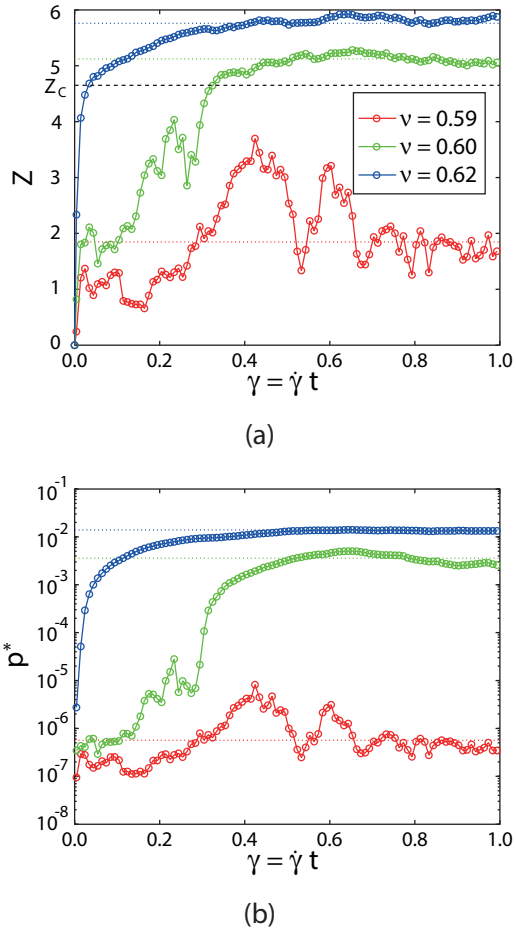

Fig. 3 Evolution of (a) the coordination number and (b) the dimensionless pressure for different values of the volume fraction when $\dot{\gamma}^* = 3.16 \cdot 10^{-5}$. Final steady state values are denoted with dotted lines; the dashed line represents the critical coordination number of Eq. (3)

3.2 Unsteady regime

The evolutions of the coordination number Z and the dimensionless pressure p^* with the accumulated shear strain γ obtained by shearing initially isotropic athermal gases are illustrated in Fig. 3(a) and (b), respectively. As previously stated, the measurements are recorded at strain intervals of 0.001. In order to smooth out the plots, a moving average of amplitude $\Delta\gamma = 0.01$ is applied a posteriori. Every 1% of strain, then, ten measurements are available and have been used to obtain mean and standard deviation of the measured quantities.

At $\gamma = 0$, a global shear rate $\dot{\gamma} = 2V/L$ is instantly applied, such that the global, dimensionless shear rate is $\dot{\gamma}^* = 3.16 \cdot 10^{-5}$. Fig. 3 shows that the coordination number and the pressure essentially increase with time until a steady state, in a statistical sense, is reached, and are closely related, as was previously observed by Sun and Sundaresan [39] in their rate-independent regime. Other quantities, such as shear stress, eigenvalues of the stress tensor and eigenvalues of the fabric tensor are measured in the simulations, although not discussed in this work, and show the attainment of the statistical steady state at approximately the same shear strain. In the case $\nu = 0.59$, large fluctuations for both p^* and Z characterize the flow, even at the steady state. This is a signal that the system is always fluid during the simulation, with large fluctuations in the coordination number due to the rapid rearrangement of the particles. The coordination number is always less than 4.6 (dashed lines in Fig. 3a), i.e., the critical coordination number for the development of rate-independent component of the stresses in steady, homogeneous shear flows (Fig. 2), but also greater than zero, indicating the presence of particle clusters. The continuing destruction and re-building of clusters gives rise to the observed large fluctuations in both coordination number and pressure (see Supplementary Movie 1).

For $\nu = 0.62$, the coordination number and the pressure smoothly increase from 0 to the steady values, with the latter one larger than that at $\nu = 0.59$ by several orders of magnitude (Fig. 3). The steady state is reached at $\gamma \approx 0.5$. Almost immediately, the coordination number is larger than 4.6, and chains of contacts span the entire domain (see Supplementary Movie 2).

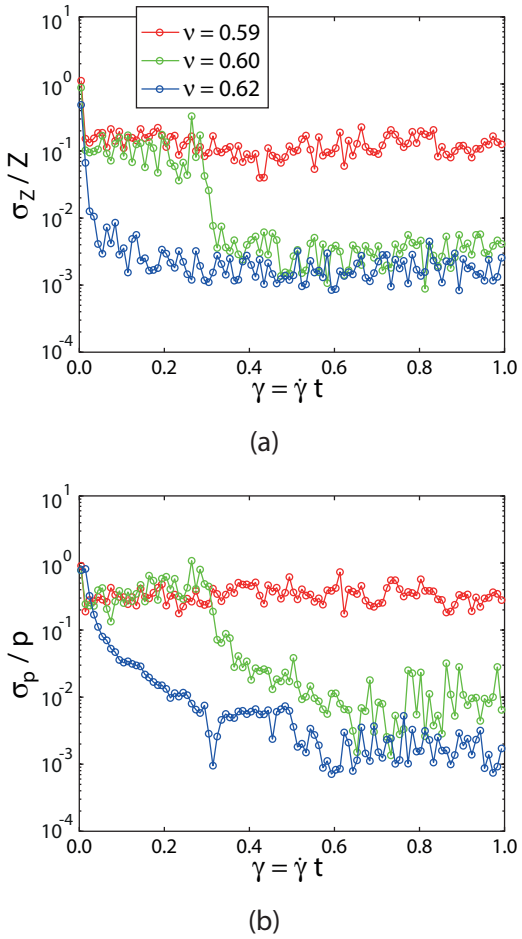

Fig. 4 Evolution of the scaled standard deviation of (a) the coordination number and (b) the dimensionless pressure for different values of the volume fraction when $\dot{\gamma}^* = 3.16 \cdot 10^{-5}$

The time required by the contact network to rearrange is responsible for a clear transient regime in terms of both Z and p^*. Once the contact network is fully developed, the very small fluctuations of Z and p^* are due to micro-structural rearrangements during shear. This is interpreted as a signature of solid behaviour. The larger the volume fraction, the smaller the fluctuations, since particles are more compacted and cannot easily abandon force chains. We point out that, even in solid conditions, no shear localization is observed and the specimens are homogeneous during the whole transient regime.

The transition from fluid to solid is evident in the case $\nu = 0.60$. There, the behaviour of Z and p^* is initially very similar to the fluid case ($\nu = 0.59$), with large fluctuations in both quantities. At $\gamma \approx 0.3$, the system experiences a significant increase in the coordination number and pressure (Fig. 3), with a corresponding decrease in the fluctuations. At $\gamma \approx 0.3$, the coordination number is approximately equal to 4.6, that is the critical value Z_c of Eq. (3).

To quantitatively characterize the fluctuations, the standard deviations of the coordination number σ_Z and pressure σ_p over the window $\Delta\gamma$, scaled by the corresponding mean quantities Z and p, as functions of γ are plotted in Fig. 4(a) and (b), respectively. When $\nu = 0.59$, the scaled amplitude of the fluctuations in the coordination number is of order 10^{-1} (Fig. 4a). For $\nu = 0.62$, both σ_Z/Z and σ_p/p are almost immediately of order of 10^{-3}. The standard deviation of each quantity is affected by the amplitude of $\Delta\gamma$. Nevertheless, σ_Z/Z and σ_p/p for $\nu = 0.62$ are always two orders of magnitude smaller than in the case $\nu = 0.59$, independent of $\Delta\gamma$. In the case $\nu = 0.60$, the scaled amplitude of the fluctuations is of order 10^{-1} when $Z < 4.6$ (fluid regime) and drops to the order of 10^{-3} (solid regime) when $Z \approx 4.6$. This analysis suggests that the same critical coordination number for the development of rate-independent components of the stresses evaluated in steady, homogeneous shear flows, and for the jamming transition of isotropic random packings, is responsible for the fluid-solid transition under unsteady, homogeneous shear flows.

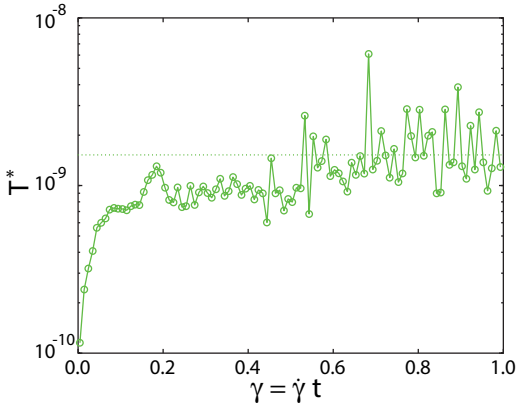

Fig. 5 Evolution of dimensionless granular temperature T^* for $\nu = 0.60$ when $\dot{\gamma}^* = 3.16 \cdot 10^{-5}$. The dotted line represents the value at steady state

Fig. 5 illustrates the evolution of the dimensionless granular temperature when $\nu = 0.60$. Unlike the pressure and the coordination number, the fluctuations of T^* are small when $Z < Z_c$ and large when $Z > Z_c$. When the granular material solidifies ($Z > Z_c$), there are force chains spanning the domain that are continuously broken and re-formed during the shear. A cascade of collisions is generated by the breaking of the force chains, resulting in strong fluctuations of granular temperature. This slightly affects the pressure because, for sufficiently rigid particles, the elastic component of the

pressure is much larger than that associated with exchange of momentum [3]. In absence of a contact network spanning the whole medium (under fluid conditions, i.e., when $Z < Z_c$), the fluctuations in the granular temperature are far less dramatic (Fig. 5), since the flow is continuously agitated.

3.2.1 Dependence on the shear rate

So far, it has been suggested that granular materials subjected to unsteady, homogeneous shearing experience a fluid-solid transition when the coordination number exceeds a critical value; and the transition has been identified by observing completely different amplitudes in the fluctuations of pressure and coordination number, at least for slow shearing and/or sufficiently rigid particles, in the two regimes. Although a criterion based on the fluctuations in the pressure has been already suggested for identifying a phase transition in the case of steady, homogeneous shearing of granular materials [8], it has also been shown that phase transition implies the development of rate-independent behaviour.

The influence of the dimensionless shear rate on the evolution of the coordination number and its fluctuations are illustrated in Figs. 6-8 for the three volume fractions investigated. Three values of the dimensionless shear rate are applied. Large values of $\dot{\gamma}^*$ are equivalent to either small particle stiffness k_n, i.e. soft particles, or rapid shearing. As is shown in Figs. 6-8, the fluctuations of the coordination number are strongly affected by the dimensionless shear rate if $Z < Z_c$ and decrease for increasing $\dot{\gamma}^*$. Conversely, the scaled fluctuations of the coordination number (and also of the pressure, not shown here for brevity) are rate-independent when $Z > Z_c$, reinforcing the idea that the fluid-solid transition takes place at $Z = Z_c$.

In the recent past, several authors showed that, under homogeneous steady shearing, pressure and granular temperature can be fitted by using asymptotic power-law relations of the shear strain, if scaled by powers of $\nu - \nu_c$, the distance to jamming in terms of volume fraction [15, 32, 33, 34, 41]. In unsteady conditions, the analysis carried out in this work suggests to replace the volume fraction with the coordination number. In fact, at values of the coordination number larger than Z_c (solid regime), Sun and Sundaresan [39] have found that

$$p^* = a_s \left(Z - Z_c\right)^2, \quad \text{if } Z > Z_c \tag{4}$$

where $a_s = 0.0073$ is a material parameter.

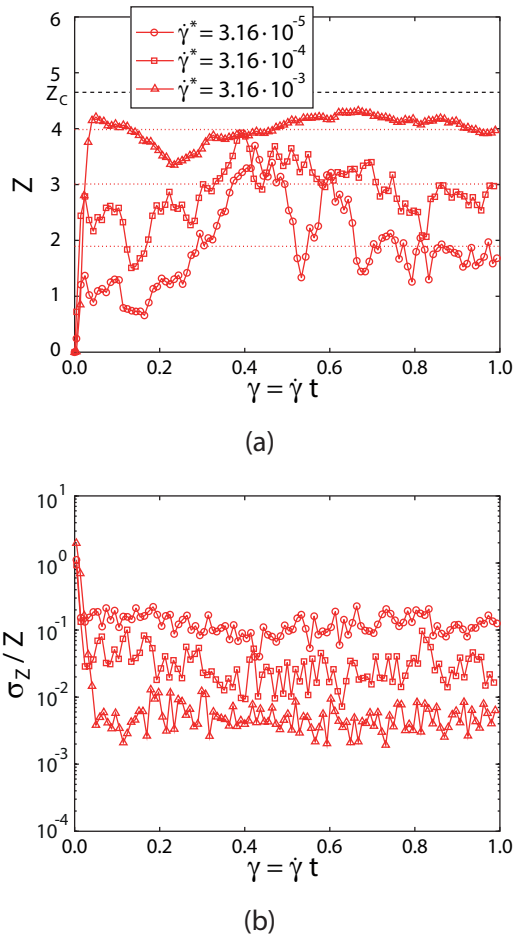

Fig. 6 Evolution of (a) the coordination number and (b) the scaled standard deviation of the coordination number for different values of the dimensionless shear rate, when $\nu = 0.59$. Steady state values are denoted with dotted lines; the dashed line represents the critical coordination number

In the fluid regime ($Z < Z_c$), the kinetic theory of granular gases [5, 12, 14, 18, 27] predicts that the pressure depends on the granular temperature. Also, p^* should diverge when the mean distance between particles is zero, at least along the direction of the principal compressive axis. This is the case when $Z = Z_c$. Then, the pressure can be assumed to be of the form

$$p^* = a_f \frac{T^{*\alpha}}{\left(Z_c - Z\right)^{\beta}}, \quad \text{if } Z < Z_c \tag{5}$$

with a_f, α and β constant coefficients. Linear regression applied to the data obtained from the present simulations when $Z < Z_c$ gives $a_f = 1.6$, $\alpha = 3/5$ and $\beta = 2$.

The collapse of the data in the two regimes can be shown by plotting $p^* / \left(Z - Z_c\right)^2$ as a function of $T^* / \left|Z - Z_c\right|^{20/3}$, as illustrated in Fig. 9(a).
Following the approach proposed by Vescovi & Luding [41], the equations describing the two scaling regimes

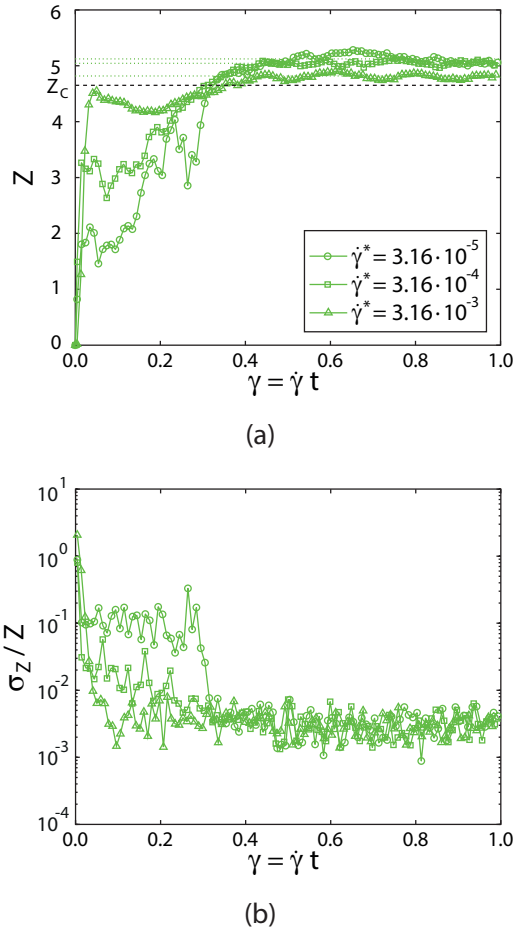

Fig. 7 Same as in Fig. 6, but when $\nu = 0.60$

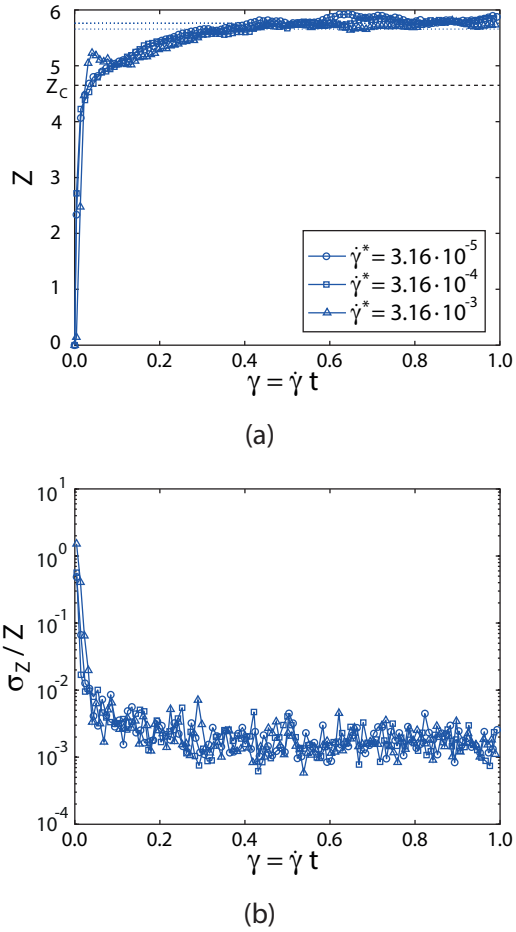

Fig. 8 Same as in Fig. 6, but when $\nu = 0.62$

Eqs. (4)-(5) can be merged into a unique function:

$$p^* = \left[\frac{a_s^{1/2} (Z - Z_c)}{2} + \right. \\ \left. + \frac{\sqrt{a_s (Z - Z_c)^2 + 4 \left(a_s a_f T^{*3/5} \right)^{1/2}}}{2} \right]^2 . \quad (6)$$

Eq. (6) is continuous and differentiable at any point, and able to predict the behaviour even at the fluid-solid transition.

As illustrated in Fig. 9(b), the granular temperature scales with the square of the dimensionless shear rate, at least for $Z < 5$. For steady shearing, the analysis of Berzi & Jenkins [3] predicts $T^*/\dot{\gamma}^{*2} = 0.53$ for $e = 0.7$ and $\mu = 0.3$, in good agreement with our measurements. By substituting this relation into Eq. (6) the dependence of p^* on Z and $\dot{\gamma}^*$ is obtained. Fig. 10 depicts the predicted dimensionless pressure (solid lines) in comparison with the results of the numerical simulations (symbols), showing a reasonable agreement.

4 Concluding remarks

The fluid-solid transition in granular materials has been investigated by performing discrete numerical simulations of unsteady, homogeneous, shear flows of identical, inelastic, soft spheres at constant volume. A constant shear rate has been instantly applied to an initially isotropic athermal gas. For a volume fraction near to the critical steady state value, fluid-solid transitions have been observed. When the rate of shear is smaller than the rate of relaxation of two particles under their repulsive potential, the fluid granular assembly exhibits fluctuations in both pressure and coordination number whose amplitude is two orders of magnitude larger with respect to the same material under solid conditions. Analogously, the fluctuations of granular temperature are particularly pronounced in the solid regime, whereas seem to disappear under fluid conditions. This can be ascribed to the presence of force chains in solid-like systems, whose micro-structural rearrangements during shear do not affect the elastic stresses, but generates a cascade of collisions resulting in strong fluctuations of

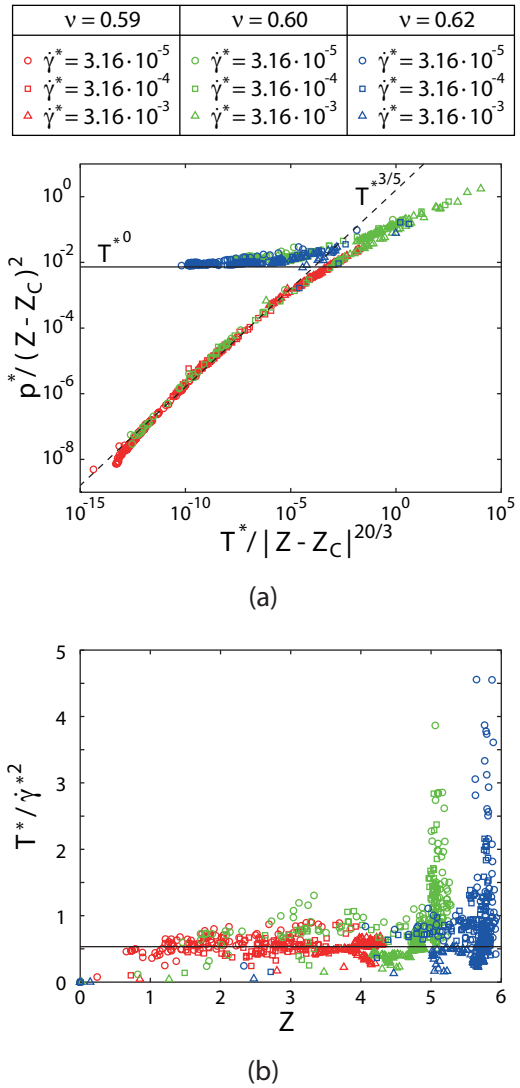

Fig. 9 (a) Collapse of dimensionless pressure plotted against dimensionless granular temperature for different dimensionless shear rates. The solid and the dashed lines represent the scaling laws in the solid (Eq. 4) and fluid regime (Eq. 5), respectively. (b) Dimensionless quantity $T^*/\dot{\gamma}^{*2}$ versus the coordination number. The solid line represents $T^*/\dot{\gamma}^{*2} = 0.53$

granular temperature. On the other hand, when the rate of shear is larger than the rate of relaxation of two particles under their repulsive potential, the difference in the fluctuation amplitude is much less evident. However, the fluctuations are rate-independent in the solid state, allowing to clearly identify the phase transition. The fluid-solid transition in unsteady, homogeneous shear flows is characterized by a critical value of the coordination number, independent of the imposed volume fraction and the shear rate. Such a critical coordination number coincides with that already defined in the past with reference to steady conditions. Finally, a constitutive relation for the pressure, valid in both fluid and solid regime, has been proposed. Such a relation involves both the coordination number and the granular temperature, suggesting that these quantities need to appear in models for the onset and the arrest of granular flows. This also implies that the coordination number should be used instead of the solid volume fraction in phase diagrams of jamming transition.

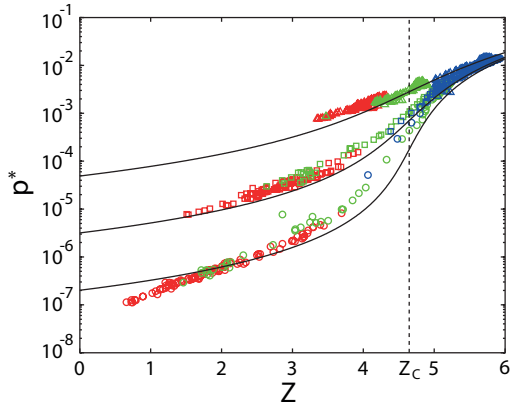

Fig. 10 Dimensionless pressure versus the coordination number for different dimensionless shear rates [see legends in Fig. 9]. The solid lines represent the proposed model Eq. (6) with $T^* = 0.53\dot{\gamma}^{*2}$

Acknowledgements Dalila Vescovi is supported by a fellowship from Fondazione Fratelli Confalonieri.

References

1. M. Alam and S. Luding. First normal stress difference and crystallization in a dense sheared granular fluid. *Phys. Fluids*, 15:2298–2312, 2003.
2. M. Babic, H.H. Shen, and H.T. Shen. The stress tensor in granular shear flows of uniform, deformable disks at high solids concentrations. *J. Fluid Mech.*, 219:81–118, 1999.
3. D. Berzi and J. Jenkins. Steady shearing flows of deformable, inelastic spheres. *Soft Matter*, 11(24): 4799–4808, 2015.
4. D. Bi, J. Zhang, B. Chakraborty, and R.P. Behringer. Jamming by shear. *Nature*, 480:355–358, 2011.
5. C.S. Campbell. Rapid granular flows. *Annu. Rev. Fluid Mech.*, 22:57–92, 1990.
6. C.S. Campbell. Granular shear flows at the elastic limit. *J. Fluid Mech.*, 465:261–291, 2002.
7. S. Chialvo and S. Sundaresan. A modified kinetic theory for frictional granular flows in dense and dilute regimes. *Phys. Fluids*, 25(7):070603, 2013.
8. S. Chialvo, J. Sun, and S. Sundaresan. Bridging the rheology of granular flows in three regimes. *Phys. Rev. E*, 85(2):021305, 2012.

9. F. da Cruz, S. Emam, M. Prochnow, J. Roux, and F. Chevoir. Rheophysics of dense granular materials: Discrete simulation of plane shear flows. *Phys. Rev. E*, 72(2):021309, 2005.
10. R. Delannay, M. Louge, P. Richard, N. Taberlet, and A. Valance. Towards a theoretical picture of dense granular flows down inclines. *Nature Mater.*, 6:99–108, 2007.
11. N. Estrada, A. Taboada, and F. Radjaï. Shear strength and force transmission in granular media with rolling resistance. *Phys. Rev. E*, 78:021301, 2008.
12. V. Garzó and J.W. Dufty. Dense fluid transport for inelastic hard spheres. *Phys. Rev. E*, 59(5):5895–5911, 1999.
13. GDR-MiDi. On dense granular flows. *Eur. Phys. J. E*, 14(4):341–365, 2004.
14. I. Goldhirsch. Rapid granular flows. *Annu. Rev. Fluid Mech.*, 35:267–293, 2003.
15. T. Hatano. Scaling properties of granular rheology near the jamming transition. *J. Phys. Soc. Jpn.*, 77 (12):123002, 2008.
16. D. Howell, R.P. Behringer, and C. Veje. Stress fluctuations in a 2d granular couette experiment: A continuous transition. *Phys. Rev. Lett.*, 82:5241–5244, 1999.
17. O.I. Imole, N. Kumar, V. Magnanimo, and S. Luding. Hydrostatic and shear behavior of frictionless granular assemblies under different deformation conditions. *KONA Powder and Particle Journal*, 30:84–108, 2013.
18. J.T. Jenkins and S.B. Savage. A theory for the rapid flow of identical, smooth, nearly elastic, spherical particles. *J. Fluid Mech.*, 130:187–202, 1983.
19. S. Ji and H.H. Shen. Characteristics of temporalspatial parameters in quasisolid-fluid phase transition of granular materials. *Chin. Sci. Bull.*, 51(6): 646–654, 2006.
20. P. C. Johnson and R. Jackson. Frictional-collisional constitutive relations for granular materials, with application to plane shearing. *J. Fluid Mech.*, 176: 67–93, 1987.
21. N. Kumar, O. I. Imole, V. Magnanimo, and S. Luding. Effects of polydispersity on the micro-macro behavior of granular assemblies under different deformation paths. *Particuology*, 12:64–79, 2014.
22. A.W. Lees and S. F. Edwards. The computer study of transport processes under extreme conditions. *J. Phys. C: Solid State Phys.*, 5(15):1921–1929, 1972.
23. A. Liu and S. Nagel. Jamming is not just cool any more. *Nature*, 396:21–22, 1998.
24. S. Luding. Introduction to discrete element methods: Basics of contact force models and how to perform the micro-macro transition to continuum theory. *Eur. J. Environ. Civil Eng.*, 12(7-8):785–826, 2008.
25. S. Luding. Granular matter: So much for the jamming point. *Nature Phys.*, 12(6):531–532, 2016.
26. S. Luding and S. McNamara. How to handle the inelastic collapse of a dissipative hard-sphere gas with the tc model granular matter. *Granular Matter*, 1 (3):113–128, 1998.
27. C.K.K. Lun. Kinetic theory for granular flow of dense, slightly inelastic, slightly rough spheres. *J. Fluid Mech.*, 223:539–559, 1991.
28. T.S. Majmudar, M. Sperl, S. Luding, and R.P. Behringer. The jamming transition in granular systems t. *Phys. Rev. Lett.*, 98(5):058001, 2007.
29. N. Mitarai and H. Nakanishi. Velocity correlations in the dense granular shear flows: Effects on energy dissipation and normal stress. *Phys. Rev. E*, 75(3): 031305, 2007.
30. V. Ogarko and S. Luding. Prediction of polydisperse hard-sphere mixture behavior using tridisperse systems. *Soft Matter*, 9(40):9530–9534, 2013.
31. C.S. O'Hern, S.A. Langer, A.J. Liu, and S.R. Nagel. Random packings of frictionless particles. *Phys. Rev. Lett.*, 88(7):075507, 2002.
32. P. Olsson and S. Teitel. Critical scaling of shear viscosity at the jamming transition. *Phys. Rev. Lett.*, 99(17):178001, 2007.
33. M. Otsuki and H. Hayakawa. Critical behaviors of sheared frictionless granular materials near the jamming transition. *Phys. Rev. E*, 80(1):011308, 2009.
34. M. Otsuki, H. Hayakawa, and S. Luding. Behavior of pressure and viscosity at high densities for two-dimensional hard and soft granular materials. *Prog. Theor. Phys. Suppl.*, 184:110–133, 2010.
35. S. B. Savage. Analyses of slow high-concentration flows of granulars. *J. Fluid Mech.*, 377:1–26, 1998.
36. L.E. Silbert. Jamming of frictional spheres and random loose packing. *Soft Matter*, 6(13):2918–2924, 2010.
37. L.E. Silbert, D. Ertas, G.S. Grest, T.C. Halsey, D. Levine, and S.J. Plimpton. Granular flow down an inclined plane: Bagnold scaling and rheology. *Phys. Rev. E*, 64(5):051302, 2001.
38. C. Song, P. Wang, and H.A. Makse. A phase diagram for jammed matter. *Nature*, 453:629–632, 2008.
39. J. Sun and S. Sundaresan. A constitutive model with microstructure evolution for flow of rate-independent granular materials. *J. Fluid Mech.*,

682:590–616, 2011.

40. A. Thornton, T. Weinhart, S. Luding, and O. Bokhove. Modeling of particle size segregation: Calibration using the discrete particle method. *Int. J. Modern Phys. C*, 23(8):1240014, 2012.
41. D. Vescovi and S. Luding. Merging fluid and solid granular behavior. *Soft Matter*, 12:8616–8628, 2016.
42. D. Vescovi, C. di Prisco, and D. Berzi. From solid to granular gases: the steady state for granular materials. *Int. J. Numer. Anal. Methods Geomech.*, 37 (17):2937–2951, 2013.
43. T. Weinhart, A. Thornton, S. Luding, and O. Bokhove. From discrete particles to continuum fields near a boundary. *Granular Matter*, 14(2): 289–294, 2012.
44. T. Weinhart, R. Hartkamp, A. Thornton, and S. Luding. Coarse-grained local and objective continuum description of three-dimensional granular flows down an inclined surface. *Phys. Fluids*, 25: 070605, 2013.